

Online cone beam reconstruction with displaced flat panel detector

Michael Manhart^a, Frank Dennerlein and Holger Kunze^b

Abstract— In 3D medical imaging, the size of the reconstructable field-of-view (FOV) is a factor that significantly defines the clinical benefit of medical X-ray systems. Due to the small detector size, the diameter of the FOV of C-arm devices is limited, but it is known that the FOV can be enlarged by using a horizontally displaced detector for data acquisition in a full rotation. For such geometries recently new reconstruction algorithms were proposed, with which the image quality of the reconstructions could be improved compared to previously known ramp filtered backprojection algorithms [3]. The proposed algorithms however require a rebinning step involving complementary rays, making an online reconstruction almost impossible. We present a new algorithm, modifying the algorithm of Kunze et. al. [4] allowing an online reconstruction.

Index Terms—displaced detector, cone-beam CT, large volume

I. INTRODUCTION

C-arm computed tomography has become an integral part of interventional radiology procedures. It is a useful tool during liver lesion embolisation to visualize feeding arteries or during drainage insertions to guide the placement of tubes [1, 2].

However, conventional C-arm devices often suffer from a limited reconstructable field of view (FOV) which prohibits the imaging of complete organs or both the target and the entry point of needle applications.

It is known that the diameter of the FOV can be almost doubled by performing an acquisition with a shifted detector in a full rotation. Various algorithms are known for this geometry:

In [3], a FDK algorithm with a specific detector weighting scheme applied before the filtering step (W-FDK) is proposed which computes an artifact-free reconstruction for the plane in which the tube moves, but for large cone angles severe artifacts occur.

These artifacts can be reduced by the algorithms proposed in [4] and [5] which are based on the reconstruction scheme introduced by Noo [6].

Compared to the differentiation backprojection filtration algorithm described in [7] these algorithms have the advantage that smaller regions in the FOV can be reconstructed in high resolution without the need of

reconstructing long stripes of the FOV to perform the Hilbert transform in the reconstruction domain.

Unlike the W-FDK algorithm, the algorithms described in [4] and [5] have the disadvantage that they require a rebinning to synthesize virtual projections of approximately double width from the original data to perform a high quality Hilbert transform. This property of the reconstruction algorithm prohibits an online reconstruction during data acquisition. However the ability of online reconstruction is an important feature for reconstruction algorithms in an interventional environment, as the result has to be available shortly after the last projection was acquired to influence the progress of the procedure.

Therefore, we have reviewed the data extension step of [4] to provide an algorithm which enables online reconstruction without the disturbing reconstruction artifacts.

II. RECONSTRUCTION ALGORITHM

A. Large Volume Cone-Beam Reconstruction Formula

This section starts with a review of the algorithm Kunze et. al. described in [4] for the reconstruction of large FOV from data acquired with a displaced, equally spaced flat panel detector. This algorithm can be described as a generalization of the fan-beam inversion formula suggested in [6] to reconstruct the x-ray linear attenuation coefficient $f(\vec{x})$ with $\vec{x} = (x, y, z)$ from the cone beam projections

$$g(\lambda, \vec{\alpha}) = \int_0^{\infty} dt f(\vec{a}(\lambda) + t\vec{\alpha}).$$

$\vec{a}(\lambda)$ is the source position parameterized by the polar angle λ and $\vec{\alpha}$ the unit vector directing from the source to the detector coordinate (u, v)

$$\vec{\alpha}(\lambda, u, v) = \frac{-D\vec{e}_w(\lambda) + u\vec{e}_u(\lambda) + v\vec{e}_v(\lambda)}{\sqrt{u^2 + v^2 + D^2}},$$

with $\vec{e}_u(\lambda)$ a unit vector in row direction, $\vec{e}_v(\lambda)$ a unit vector in column direction and $\vec{e}_w(\lambda)$ a unit vector orthogonal to the detector, see figure 1. The detector coordinate $(0, 0)$ corresponds to the orthogonal projection of the source point onto the detector. The distance between detector and source is D .

In the following we assume that the detector is displaced in positive u direction. The detector could be totally displaced in one direction, so that only data for $u \geq 0$ is considered. But for stability reasons, we use a small overlap $2u_\epsilon$ so that $g(\lambda, u, v)$ is measured in the interval $[-u_\epsilon; u_m]$.

^a M. Manhart: Pattern Recognition Lab, University of Erlangen-Nuremberg, Martensstraße 3, 91058 Erlangen, Germany

^b F. Dennerlein, H. Kunze: Siemens Healthcare, 91301 Forchheim, Germany. E-Mail: holger.hk.kunze@siemens.com.

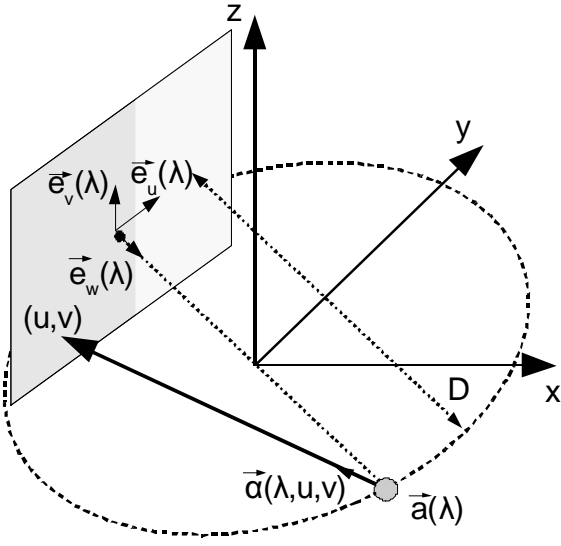


Fig. 1: Illustration of the cone-beam geometry

Given a set of such projection data, the object density can be obtained according to [4] as follows:

1. Compute the extended projection using the rebinning formula

$$g_E(\lambda, \bar{\alpha}(\lambda, u, v)) = \begin{cases} g(\lambda_E, \bar{\alpha}(\lambda_E, -u, v)), & u < -u_\epsilon \\ g(\lambda, \bar{\alpha}(\lambda, u, v)) & , u \geq -u_\epsilon \end{cases}$$

with

$$\lambda_E = \lambda + \pi - 2 \tan^{-1} \frac{u}{D}$$

2. Calculate the partial derivative of the extended data with respect to the parameter of the source trajectory

$$g_D(\lambda, u, v) = \left. \frac{d}{d\mu} g_E(\mu, \bar{\alpha}(\lambda, u, v)) \right|_{\mu=\lambda}$$

3. Multiply the differentiated data with a length correction weight

$$g_C(\lambda, u, v) = g_D(\lambda, u, v) \frac{D}{\sqrt{D^2 + u^2 + v^2}}$$

4. Perform a Hilbert transform

$$q_m(\lambda, \hat{u}, \hat{v}) = \int_{-\infty}^{\infty} d\tilde{u} h(u - \tilde{u}) g_C(\lambda, \tilde{u}, v)$$

Multiply the Hilbert transformed data with a smooth weighting function to suppress artifacts due to the data extension.

$$g_W(\lambda, u, v) = g_F(\lambda, u, v) w(\lambda, u)$$

$$w(\lambda, u) = \begin{cases} 0 & u < -u_\epsilon \\ \sin^2 \left(\frac{u + u_\epsilon}{4u_\epsilon} \pi \right) & -u_\epsilon \leq u \leq u_\epsilon \\ 1 & u > u_\epsilon \end{cases}$$

5. Back project the filtered data using a linear distance weighting

$$f(\bar{x}) = \frac{1}{2\pi} \int_{-\pi}^{\pi} d\lambda \frac{g_W(\lambda, u^*, v^*)}{(\bar{a}(\lambda) - \bar{x}) \bar{e}_w(\lambda)}$$

where (u^*, v^*) are the coordinates of the cone beam projection of \bar{x} onto the detector.

B. Separate reconstruction of measured and extended data

To achieve the goal of online reconstruction, it is necessary to process the measured data of a projection and its data extension separately, each at the moment when they can be retrieved.

For that reason the extended projection $g_E(\lambda, u, v)$ needs to be written as a linear combination of the measured data $g(\lambda, u, v)$ and the data extension $g_e(\lambda, u, v)$

$$g_E(\lambda, u, v) = \phi(\lambda, u, v) g(\lambda, u, v) + (1 - \phi(\lambda, u, v)) g_e(\lambda, u, v)$$

with $\phi(\lambda, u, v)$ a weighting function blending from the original data to the data extension. In the above reviewed algorithm $\phi(\lambda, u, v)$ is the Heaviside step function in the parameter u shifted by $-u_\epsilon$.

Due to the linearity of the reconstruction algorithm we can process both components of $g_E(\lambda, u, v)$ separately obtaining the volumes $f_m(\bar{x})$ of the measured projections and $f_e(\bar{x})$ of the projection extension.

C. Approximate data extension

In the algorithm described in section A, the data extension was done using a rebinning formula. This algorithm guarantees for the plane $z = 0$ an artifact free reconstruction, but is suboptimal with respect to computational effort and memory requirements: To be able to extend one projection several complementary projections are required.

Therefore, we propose a different data extension scheme. Due to the large extend of truncation and due to the fact that many high frequent structures are typically located at the position of truncation in such a geometry, the commonly used data extension algorithms based on the fitting of the projections of circles or ellipses are not good choices [8].

In our case, however, we can make use of the additional knowledge about the object structure contained in the opposite projections. We thus propose to use the data acquired at the position $\lambda + \pi$ to extend the current projection. This extension can then be written as

$$g_e(\lambda, u, v) = g(\lambda + \pi, -u, v).$$

Thus only data from one single projection is used for the projection extension.

Of course, this approach yields only a coarse approximation of the missing projection data. Note, however, that the extended data values are only required for the Hilbert filtering and not used during backprojection, so that the impact on image quality caused by this approximation is very low.

D. Online reconstruction algorithm

Using the linearity property of the reconstruction algorithm described in section B and the approximate data extension proposed in section C we propose the following online algorithm for a large FOV reconstruction using a displaced detector:

First, the reconstruction algorithm of section A is applied for the weighted projection $\phi(\lambda, u, v)g(\lambda, u, v)$ skipping step 1. Thus only the measured data for the projection at source position $\vec{a}(\lambda)$ are processed.

In a second step, the same projection data are flipped to obtain the projection extension $g_e(\lambda - \pi, u, v)$ for the complementary source position $\vec{a}(\lambda - \pi)$. Note that λ is a polar angle and thus $\vec{a}(\lambda)$ is a 2π periodic function. After weighting with $(1 - \phi(\lambda - \pi, u, v))$, they are processed once again by the algorithm of section A without step 1, but this time using the geometry of the source position $\vec{a}(\lambda - \pi)$.

For $\phi(\lambda, u, v)$, a cosine square function is chosen, ramping down from 1 to 0 within the range from $[-u_e; 0]$.

III. NUMERICAL EVALUATION

We compared our new algorithm of section II D to the algorithm that has been suggested in [4].

In both algorithms, we implemented the differentiation (step 3) according to the scheme described in [9]. The Hilbert transform was computed using the half pixel shift formula; see for instance [10].

As test object we chose the Schaller head phantom [11]. Cone beam projections were simulated using the parameters listed in table 1.

source isocenter distance	$R = 570$ mm
source detector distance	$D = 1200$ mm
detector pixel size	$\Delta u = \Delta v = 1$ mm
# of projections	720
overlap	$u_e = 25$ mm

Table 1: Geometry parameters used for data simulation

Figure 2 presents two slices (at $z = 0$ cm and $z = -2.4$ cm) through the reconstructions of the head phantom. Note that the visible stripes are a result of the low number of the projections and are not caused by the displaced detector.

Additionally to simulation studies we compared the reconstruction result using scanned phantoms. In figure 3 the reconstruction result of an abdomen phantom is shown.

IV. CONCLUSION

We presented a new algorithm for full scan cone beam reconstruction using a displaced detector. The results are comparable to these of the algorithm described in [4] however the new algorithm enables an online reconstruction of the investigated object. This property is gained for the computational cost of one additional back projection; however the rebinning step could be skipped which allows online reconstruction, eases data handling and reduces memory requirements.

REFERENCES

- [1] B.C. Meyer, B.B. Frericks, M. Voges, M. Borchert, P. Martus, J. Justiz, K.-J. Wolf and F. K. Wacker: "Visualization of Hypervascular Liver Lesions During TACE: Comparison of Angiographic C-Arm CT and MDCT", *AJR*, 190: W263 - W269, 2008
- [2] C.Becker, T. Wagnershauser, K. Krimmel, G. Michalski, U. Lechel, O. Meissner: "LARGE VOLUME C-arm CT: Liver Coverage, Image Quality, and Radiation Exposure", *RSNA 2008*, SSJ24-02
- [3] G. Wang: "X-ray micro-CT with a displaced detector array", *Med. Phys.* 29 (7), pp. 1634 – 1636, Jul. 2002
- [4] H. Kunze, M. Manhart, F. Dennerlein: " Cone beam reconstruction with displaced flat panel detector", *Proc. Int. Conf. Fully 3D Image Reconstruction*, pp 138-145
- [5] D. Schäfer, M. Grass: " Cone-beam filtered back-projection for circular X-ray tomography with off-centerdetector", *Proc. Int. Conf. Fully 3D Image Reconstruction*, pp 86-89
- [6] F. Noo , M. Defrise, R. Clackdoyle, H. Kudo: "Image reconstruction from fan-beam projections on less than a short-scan", *Phys. Med. Biol.* 47, pp. 2525-2546, 2002
- [7] S. Leng, T. Zhuang, BE. Nett, GH. Chen, *Phys. Med. Biol.*, Vol. 50, 1805–20, 2005.
- [8] J. Hsieh, E. Chao, J. Thibault, B. Grekowicz, A. Horst, S. McOlash, T.J. Myers: "A novel reconstruction algorithm to extend the CT scan field-of-view." *Med. Phys.* 31 (9), pp. 2385-2391, 2004
- [9] F. Noo, S. Hoppe, F. Dennerlein, G. Lauritsch, J. Hornegger: "A new scheme for view-dependent data differentiation in fan-beam and cone-beam computed tomography", *Phys. Med. Biol.*, Vol 52, pp. 5393-5414, 2007
- [10] F. Noo, J. D. Pack, D. Heuscher: "Exact helical reconstruction using native cone-beam geometries." *Phys. Med. Biol.*, Vol 48, pp. 3787-3818, 2003
- [11] S. Schaller, Th. Flohr, P. Steffen: "An Efficient Fourier Method for 3-D Radon Inversion in Exact Cone-Beam CT Reconstruction", *IEEE Transactions on Medical Imaging*, Vol. 17 (2), pp. 244-250, Apr. 1998

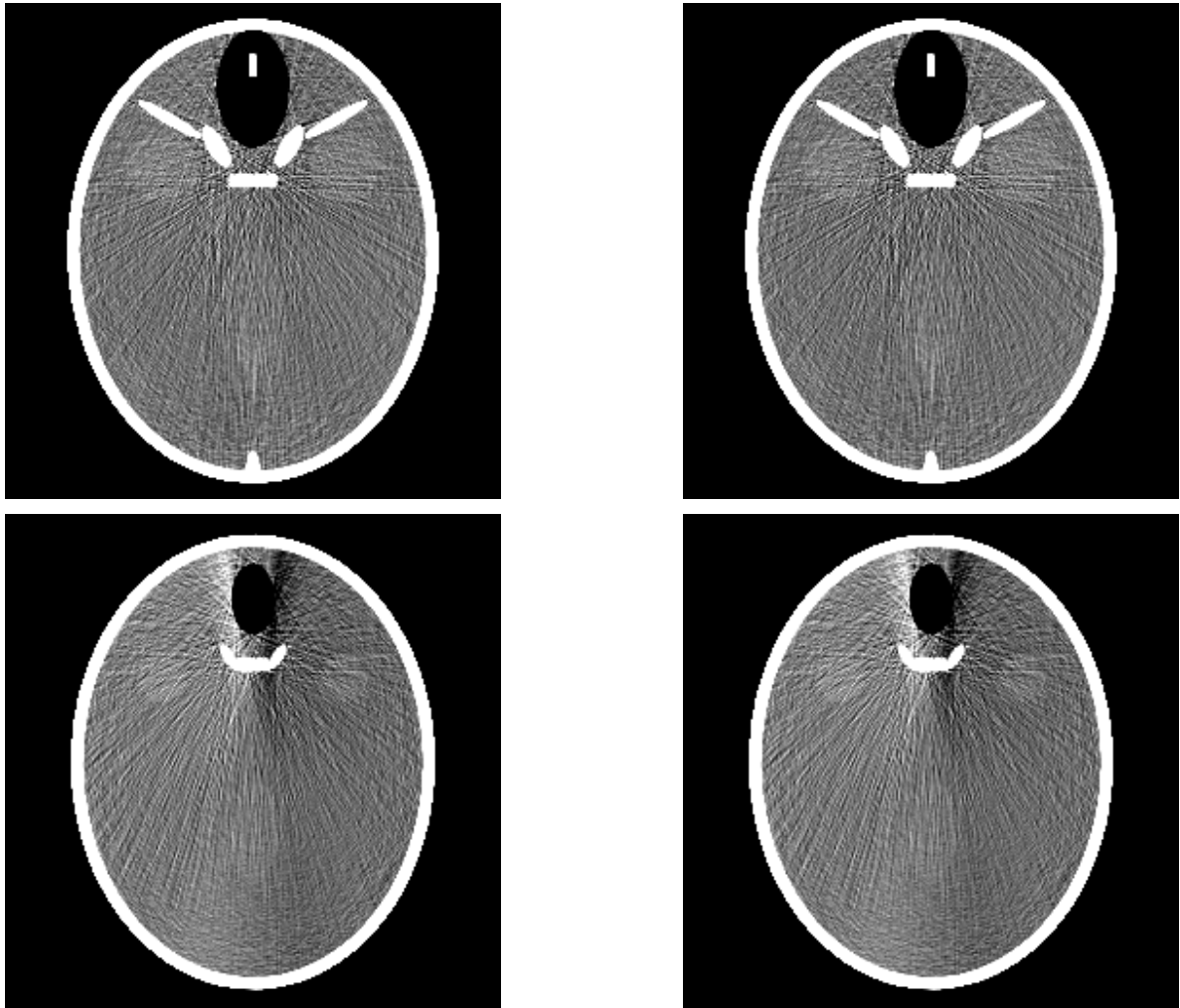


Fig. 2: Comparison of the reconstruction result using the proposed method (left) and method proposed in [4] (right) for $z = 0$ cm (top) and $z = -2.4$ cm (bottom) in the gray scale window [-100 HU; 100 HU]

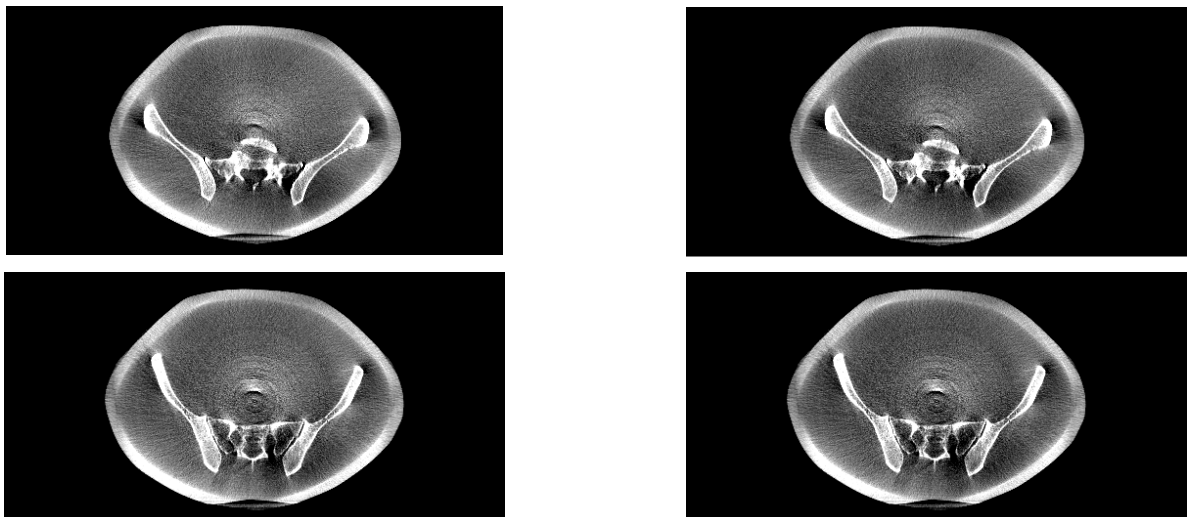


Fig. 3: Comparison of the reconstruction result using the proposed method (left) and method proposed in [4] (right) for $z = 0$ cm (top) and $z = -2$ cm (bottom) in the gray scale window [-200 HU; 400 HU]